

Gravitational waves from a scotogenic two-loop neutrino mass model

Cesar Bonilla,^a A. E. Cárcamo Hernández,^b João Gonçalves,^{c,d}
Vishnudath K. N.,^b António P. Morais^{c,e} and Roman Pasechnik^d

^aDepartamento de Física, Universidad Católica del Norte,
Avenida Angamos 0610, Casilla 1280, Antofagasta, Chile

^bUniversidad Católica del Norte and Centro Científico-Tecnológico de Valparaíso,
Casilla 110-V, Valparaíso, Chile

^cDepartamento de Física da Universidade de Aveiro and Centre for Research and Development in
Mathematics and Applications (CIDMA),
Campus de Santiago, 3810-183 Aveiro, Portugal

^dDepartment of Physics, Lund University,
221 00 Lund, Sweden

^eTheoretical Physics Department, CERN,
1211 Geneva 23, Switzerland

E-mail: cesar.bonilla@ucn.cl, antonio.carcamo@usm.cl, jpedropino@ua.pt,
vishnudath.neelakand@usm.cl, aapmoraais@ua.pt, roman.pasechnik@hep.lu.se

Abstract. We propose a framework to account for neutrino masses at the two-loop level. This mechanism introduces new scalars and Majorana fermions to the Standard Model. It is assumed the existence of a global $U(1) \times \mathbb{Z}_2$ symmetry which after partial breaking provides the stability of the dark matter candidates of the theory. The rich structure of the potential allows for the possibility of first-order phase transitions (FOPTs) in the early Universe which can lead to the generation of primordial gravitational waves as one of the potentially observable signatures of this model. Taking into account relevant constraints from lepton flavour violation, neutrino physics as well as the trilinear Higgs couplings at next-to-leading order accuracy, we have found a wide range of possible FOPTs which are strong enough to be probed at the proposed gravitational-wave interferometer experiments such as LISA.

Contents

1	Introduction	1
2	Theoretical structure of the model	2
2.1	Particle content and charge assignments	2
2.2	Yukawa sector and scalar potential	3
2.3	Scalar mass spectrum	4
2.4	Implications for collider physics and Dark Matter phenomenology	5
3	Neutrino mass and lepton flavor violation	6
4	Phase transitions and primordial gravitational waves	9
4.1	Numerical results	12
5	Conclusions	15
A	One-loop expression for the physical trilinear Higgs coupling	16

1 Introduction

The Standard Model (SM) is a highly successful theory that describes the strong, electromagnetic, and weak interactions whose predictions have been experimentally verified at the LHC with the highest degree of accuracy. However it has several unaddressed issues such as, the observed pattern of SM fermion masses and mixing angles, the number of SM fermion families, the measured amount of Dark Matter (DM) relic density and baryon asymmetry observed in the Universe, among others. Experiments with solar, atmospheric, and reactor neutrinos have brought evidence of neutrino oscillations as a signature of their nonzero masses and mixing. Several extensions of the SM have been constructed in order to explain the tiny masses of the active neutrinos; see for instance Ref. [1] for a review.

The most economical way to generate the small neutrino masses considering the SM gauge symmetry is by adding two right-handed Majorana neutrinos that mix with the light active neutrinos thus triggering a type-I seesaw mechanism [2–8]. In this mechanism, either the right-handed Majorana neutrinos have to be extremely heavy, with masses of order the Grand Unification scale, or they can be around the TeV scale implying very tiny Dirac Yukawa couplings, in order to successfully reproduce the neutrino data. In both scenarios, the mixing between the active and sterile neutrinos is very small, making the detection at the collider experiments difficult and strongly suppressed charged lepton flavor violating (LFV) signatures, several orders of magnitude below the experimental sensitivity. This makes models with tree-level type-I seesaw realizations difficult to test at the particle physics experiments.

Alternatively, radiative seesaw models are examples of interesting and testable extensions of the SM naturally explaining tiny neutrino masses and the absence of a strong hierarchy between the neutrino mixing angles. In most radiative seesaw models, neutrino masses arise at a one-loop level. This implies that in order to successfully reproduce the experimental neutrino data, one has to rely either on very small neutrino Yukawa couplings (of order the electron Yukawa coupling) or on an unnaturally small mass splitting between the CP-even and CP-odd components of the neutral scalar mediators. Two-loop neutrino mass models have been proposed in the literature [9–17] to naturally provide further suppressed active neutrino masses than those based on one-loop level radiative seesaw mechanisms. See [18, 19] for comprehensive studies of one- and two-loop neutrino mass models.

Our goal here is to explore a particularly attractive new scenario for neutrino mass generation at the two-loop level based upon an additional global $U(1) \times \mathcal{Z}_2$ symmetry in the lepton sector, featuring also inert scalars and heavy Majorana neutrinos. Among the most promising phenomenological signatures of this model are the emergence of strong first-order phase transitions (FOPTs) that can be studied via a possible detection of a stochastic gravitational wave background (SGWB) as well as a sizeable modification in the trilinear Higgs coupling that can be probed at the LHC and future colliders. In this work, we study intricate correlations among these signatures and the properties of the neutrino sector.

The paper is organised as follows. In Sec. 2, we introduce our model with a focus on the Yukawa and scalars sectors; in Sec. 3 we discuss the phenomenological implications of the new additional states in the context of neutrino physics and charged LFV observables; in Sec. 4 we introduce the main building blocks for the finite-temperature description of our model and how it can be correlated with SGWB observables, also showcasing our numerical results; finally, we finish with Sec. 5 where we take our conclusions.

2 Theoretical structure of the model

2.1 Particle content and charge assignments

In this work, we augment the SM gauge groups with an extended global abelian symmetry $U(1) \times \mathcal{Z}_2$, where the $U(1)$ is spontaneously broken while the \mathcal{Z}_2 is preserved. Besides the standard particle content of the SM, additional fields are present in the spectrum, including an inert $SU(2)$ doublet scalar field, η , and two scalar singlets, φ and σ . In our setup, σ acquires a nonzero vacuum expectation value (VEV) while φ does not, such that the potential DM candidates can arise from the neutral components of η or from φ . Additional Majorana fermions are also included into this scheme, namely, two N_R fields and two Ψ_R . While the electroweak (EW) gauge group does not distinguish N_R and Ψ_R , the extended symmetry group treats both differently.

The charge assignments of the fields are shown in Tab. 1 for the scalar fields and in Tab. 2 for matter fields. As shown in Tab. 1, the $SU(2)$ scalar doublet η and the scalar singlet φ have non-trivial \mathcal{Z}_2 charges. Since these two scalars do not acquire VEVs and the charge assignments do not let neutrinos to couple to the SM Higgs, light active neutrinos do not acquire masses at tree level. The specific $U(1) \times \mathcal{Z}_2$ charge assignments of the $N_{k,R}$ Majorana neutrinos and σ scalar field enables the radiative generation of neutrino mass and the corresponding mixing only at two-loop level that can be noticed from a typical topology in Fig. 1. Namely, this is possible through the virtual exchange of the neutral components of the inert $SU(2)$ scalar doublet η fields as well as of the real and imaginary parts of the inert singlet scalar φ , with the loop closing through the σ VEV and the VEV of the active Higgs doublet Φ . For simplicity of the analysis, we assume that the charged lepton sector is purely diagonal, such that the only contribution to the Pontecorvo–Maki–Nakagawa–Sakata (PMNS) mixing matrix comes exclusively from the loop topology shown in Fig. 1.

	$SU(3)_C$	$SU(2)_L$	$U(1)_Y$	$U(1)_X$	\mathcal{Z}_2
Φ	1	2	1/2	0	1
σ	1	1	0	-1/2	1
η	1	2	1/2	0	-1
φ	1	1	0	-1/2	-1

Table 1: Charge assignments under the SM gauge group ($SU(3)_C \times SU(2)_L \times U(1)_Y$) and the supplemental global symmetry $U(1)_X \times \mathcal{Z}_2$ for the new scalar fields (σ , η and φ) and the Higgs doublet (Φ).

	$SU(3)_C$	$SU(2)_L$	$U(1)_Y$	$U(1)_X$	\mathcal{Z}_2
$\ell_{i,L}$	1	2	$-1/2$	$1/2$	1
$\ell_{i,R}$	1	1	-1	$1/2$	1
$N_{k,R}$	1	1	0	$1/2$	-1
$\Psi_{k,R}$	1	1	0	0	1

Table 2: Charge assignments under the SM gauge group $(SU(3)_C \times SU(2)_L \times U(1)_Y)$ and the supplemental global symmetry $U(1)_X \times \mathcal{Z}_2$ for the new matter fields (N_R, Ψ_R) and the SM-like lepton doublet $(\ell_{i,L})$ and singlet $(\ell_{i,R})$. Here, $i = 1, 2, 3$ and $k = 1, 2$.

2.2 Yukawa sector and scalar potential

Based on the charge assignments of Tabs. 1 and 2, the most general and renormalisable Yukawa Lagrangian reads as

$$-\mathcal{L}_Y^{(l)} = (y_\ell)_{ij} \bar{\ell}_{i,L} \Phi \ell_{j,R} + (y_N)_{ik} \bar{\ell}_{i,L} \tilde{\eta} N_{k,R} + (y_\Omega)_{nk} \bar{N}_{n,R} \varphi^* \Psi_{k,R}^c + (m_\Psi)_{nm} \bar{\Psi}_{n,R} \Psi_{m,R}^c + \text{h.c.}, \quad (2.1)$$

where we have defined $\tilde{\eta} = i\sigma_2 \eta^\dagger$ and the superscript c in the Ψ field indicates charge conjugation. We adopt the Einstein summation convention where repeated indices indicate sum over them, with $i, j = 1, 2, 3$ and $m, n, k = 1, 2$. Here, y_ℓ is a 3×3 matrix, y_Ω and m_ψ are 2×2 matrices and y_N is a 2×3 matrix. The neutrino mass matrix can then be induced by the combination of the y_N and y_Ω Yukawa matrices.

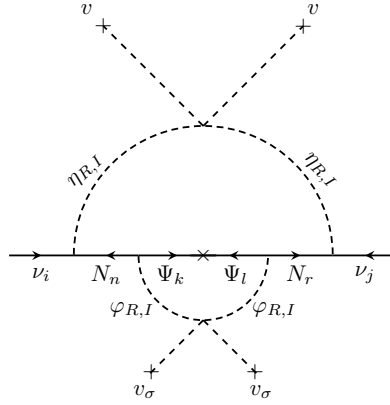


Figure 1: Two-loop Feynman diagram which is responsible for the generation of the neutrino masses and mixing. Here, ν are the neutrinos, $\eta_{R,I}$ are the real and imaginary parts of the neutral component of the η doublet, $\varphi_{R,I}$ are the real and imaginary parts of the φ singlet, v and v_σ are the VEVs of the Φ doublet the σ singlet fields, respectively.

The complete gauge invariant scalar potential in this model is given as,

$$\begin{aligned} V = & -\mu_\Phi^2 (\Phi^\dagger \Phi) + \mu_\eta^2 (\eta^\dagger \eta) + \mu_\varphi^2 (\varphi^* \varphi) - \mu_\sigma^2 (\sigma^* \sigma) - \mu_{sb}^2 (\sigma^2 + \text{h.c.}) + \lambda_1 (\Phi^\dagger \Phi) (\Phi^\dagger \Phi) + \lambda_2 (\eta^\dagger \eta) (\eta^\dagger \eta) \\ & + \lambda_3 (\varphi^* \varphi) (\varphi^* \varphi) + \lambda_4 (\sigma^* \sigma) (\sigma^* \sigma) + \lambda_5 (\Phi^\dagger \Phi) (\eta^\dagger \eta) + \lambda_6 (\Phi^\dagger \eta) (\eta^\dagger \Phi) + \frac{\lambda_7}{2} [(\Phi^\dagger \eta)^2 + \text{h.c.}] \\ & + \lambda_8 (\Phi^\dagger \Phi) (\sigma^* \sigma) + \lambda_9 (\Phi^\dagger \Phi) (\varphi^* \varphi) + \lambda_{10} (\eta^\dagger \eta) (\sigma^* \sigma) + \lambda_{11} (\eta^\dagger \eta) (\varphi^* \varphi) + \lambda_{12} (\varphi^* \varphi) (\sigma^* \sigma) \\ & + \frac{\lambda_{13}}{2} [\varphi^2 (\sigma^*)^2 + \text{h.c.}], \end{aligned}$$

where we take all parameters of the potential to be real, i.e. CP symmetry is conserved in the considered scenario. Notice that the quartic couplings λ_7 and λ_{13} are crucial for generating neutrino

masses through out the two-loop level mechanism. The nonzero scalar VEVs are denoted as $\langle \Phi \rangle = v \sim 246$ GeV and $\langle \sigma \rangle = v_\sigma$. Also, the term μ_{sb}^2 that breaks the $U(1)_X$ symmetry softly is incorporated in order to make the CP-odd scalar associated with σ massive. Once the scalars Φ and σ acquire VEVs and the EW symmetry is broken, the model will have nine physical scalars – two charged scalars (η^\pm), four neutral CP-even scalars (η_R , φ_R , h_1 and h_2) and three neutral CP-odd scalars (η_I , φ_I and σ_I). It is to be noted that the scalars associated with η and φ mix only among themselves and so do the scalar fields coming from Φ and σ ¹.

2.3 Scalar mass spectrum

After employing the minimization conditions along v and v_σ , the scalar mass matrices can be written as

$$\begin{aligned}
M_{\eta^\pm}^2 &= \begin{pmatrix} 0 & 0 & 0 & 0 \\ 0 & 0 & 0 & 0 \\ 0 & 0 & \mu_\eta^2 + \frac{v_\sigma^2 \lambda_{10} + v^2 \lambda_5}{2} & 0 \\ 0 & 0 & 0 & \mu_\eta^2 + \frac{v_\sigma^2 \lambda_{10} + v^2 \lambda_5}{2} \end{pmatrix}, \\
M_{\text{CP-even}}^2 &= \begin{pmatrix} 2v^2 \lambda_1 & vv_\sigma \lambda_8 & 0 & 0 \\ vv_\sigma \lambda_8 & 2v_\sigma^2 \lambda_4 & 0 & 0 \\ 0 & 0 & \mu_\eta^2 + \frac{v_\sigma^2 \lambda_{10} + v^2 \lambda_5 + v^2 \lambda_6 + \lambda_7 v^2}{2} & 0 \\ 0 & 0 & 0 & \mu_\varphi^2 + \frac{v_\sigma^2 \lambda_{12} + v_\sigma^2 \lambda_{13} + v^2 \lambda_9}{2} \end{pmatrix}, \\
M_{\text{CP-odd}}^2 &= \begin{pmatrix} 0 & 0 & 0 & 0 \\ 0 & 4\mu_{sb}^2 & 0 & 0 \\ 0 & 0 & \mu_\eta^2 + \frac{v_\sigma^2 \lambda_{10} + v^2 \lambda_5 + v^2 \lambda_6 - v^2 \lambda_7}{2} & 0 \\ 0 & 0 & 0 & \mu_\varphi^2 + \frac{v_\sigma^2 \lambda_{12} - v_\sigma^2 \lambda_{13} + v^2 \lambda_9}{2} \end{pmatrix}, \tag{2.2}
\end{aligned}$$

where the zero-eigenvalues of the charged and CP-odd matrices are absorbed by the longitudinal components of the W^\pm and Z^0 gauge bosons. To avoid constraints coming from the Higgs sector, we work closely to the alignment limit, such that $vv_\sigma \lambda_8 \ll 1$. The above matrices can be analytically

¹Let us note that similar scalar potentials can be found in scenarios that explain Dirac neutrino masses at the one-loop level [20]. A detailed investigation of such scenarios, following the lines of the present work, will be dedicated in a subsequent paper.

diagonalised, which results in the mass eigenvalues

$$\begin{aligned}
& \text{Charged scalars : } \left\{ m_{\eta^\pm}^2 = \mu_\eta^2 + \frac{1}{2} (\lambda_5 v^2 + \lambda_{10} v_\sigma^2) \right. \\
& \text{CP - even scalars : } \left\{ \begin{aligned} m_{h_1}^2 &= \lambda_1 v^2 + \lambda_4 v_\sigma^2 - \sqrt{(\lambda_1 v^2 - \lambda_4 v_\sigma^2)^2 + \lambda_8^2 v^2 v_\sigma^2}, \\ m_{h_2}^2 &= \lambda_1 v^2 + \lambda_4 v_\sigma^2 + \sqrt{(\lambda_1 v^2 - \lambda_4 v_\sigma^2)^2 + \lambda_8^2 v^2 v_\sigma^2}, \\ m_{\eta_R}^2 &= \mu_\eta^2 + \frac{1}{2} (v^2 (\lambda_5 + \lambda_6 + \lambda_7) + \lambda_{10} v_\sigma^2), \\ m_{\varphi_R}^2 &= \mu_\varphi^2 + \frac{1}{2} (\lambda_9 v^2 + v_\sigma^2 (\lambda_{12} + \lambda_{13})). \end{aligned} \right. \\
& \text{CP - odd scalars : } \left\{ \begin{aligned} m_{\sigma_I}^2 &= 4\mu_{sb}^2, \\ m_{\eta_I}^2 &= \mu_\eta^2 + \frac{1}{2} (v^2 (\lambda_5 + \lambda_6 - \lambda_7) + \lambda_{10} v_\sigma^2), \\ m_{\varphi_I}^2 &= \mu_\varphi^2 + \frac{1}{2} (\lambda_9 v^2 + v_\sigma^2 (\lambda_{12} - \lambda_{13})). \end{aligned} \right.
\end{aligned} \tag{2.3}$$

Here, the lightest scalar m_{h_1} is taken to be the SM Higgs boson of mass ~ 125 GeV. The above expressions can be inverted to express 7 out of the 13 quartic couplings in terms of the physical scalar masses. Thus, the physical masses can be taken as the input parameters in the numerical analysis. The relations that are used in this work are,

$$\begin{aligned}
\lambda_1 &= \frac{m_{h_1}^2 - \sqrt{(m_{h_1}^4 - 2m_{h_2}^2 m_{h_2}^2 + m_{h_2}^4 - 4\lambda_8^2 v_1^2 v_\sigma^2)} + m_{h_2}^2}{4v_1^2} \\
\lambda_4 &= \frac{m_{h_1}^2 + \sqrt{(m_{h_1}^4 - 2m_{h_1}^2 m_{h_2}^2 + m_{h_2}^4 - 4\lambda_8^2 v_1^2 v_\sigma^2)} + m_{h_2}^2}{4v_\sigma^2} \\
\lambda_5 &= \frac{-2\mu_\eta^2 + 2m_{\eta^\pm}^2 - \lambda_{10} v_\sigma^2}{v_1^2} \\
\lambda_6 &= \frac{m_{\eta_I}^2 + m_{\eta_R}^2 - 2m_{\eta^\pm}^2}{v_1^2} \\
\lambda_7 &= \frac{-m_{\eta_I}^2 + m_{\eta_R}^2}{v_1^2} \\
\lambda_9 &= \frac{-2\mu_{sb}^2 + m_{\eta_I}^2 + m_{\eta_R}^2 - v_\sigma^2 \lambda_{12}}{v_1^2} \\
\lambda_{13} &= \frac{m_{(\varphi)_R}^2 - m_{(\varphi)_I}^2}{2v_\sigma^2}
\end{aligned} \tag{2.4}$$

2.4 Implications for collider physics and Dark Matter phenomenology

Finally, to close this section we wish to provide a brief discussion of the key phenomenological implications of the multi-scalar sector in the considered model. It is expected that the presence of electrically charged scalars in the inert doublet will provide an extra contribution to the Higgs diphoton decay rate $h \rightarrow \gamma\gamma$, which will yield a deviation of the Higgs diphoton signal strength from the SM expectation. However, that deviation is expected to occur in the experimentally allowed range in a large region of the model parameter space. Besides, given that the singlet scalar field acquires a VEV at the TeV scale, its mixing with the CP-even part of the active doublet is suppressed implying that the couplings of the 125 GeV SM like Higgs boson will be very close to the SM expectation realising the so-called Higgs alignment limit. Thus, such a scenario appears to be consistent with the SM in such a limit, at least, at the leading order (LO) level.

It is generally expected that the triple Higgs coupling can be affected compared to its SM value in multi-scalar extensions of the SM. In this study, the trilinear Higgs coupling, λ_{hhh} , deviates from the SM prediction through a mixing with the σ field. In particular, at LO, a simple analytical expression is obtained and reads as

$$\lambda_{hhh}^{\text{LO}} = 6 \cos^3 \alpha_h v \lambda_1 + 6 \sin^3 \alpha_h v_\sigma \lambda_4 + 3 \cos \alpha_h \sin^2 \alpha_h v \lambda_8 + 3 \cos^2 \alpha_h \sin \alpha_h v_\sigma \lambda_8, \quad (2.5)$$

where α_h is the CP-even mixing angle between h_1 (Higgs) and h_2 . It is not hard to notice that in the limit of $\alpha_h \rightarrow 0$, the tree-level SM Higgs coupling $\lambda_{hhh}^{\text{SM}} = 6v\lambda_1$ is successfully reproduced as we effectively work very close to the alignment limit. Hence, the potential corrections to $\lambda_{hhh}^{\text{LO}}$ are very suppressed and we expect no significant deviations from the SM expectation. On the other hand, previous works [21–23] have suggested that one-loop corrections to the λ_{hhh} can actually be quite sizable in some BSM extensions, resulting, in some cases, in an increase of order $\mathcal{O}(50\%)$ for certain combinations coupling/mass parameters. In our case, next-to-leading order (NLO) contributions will be dominant and represent the bulk of the new physics contribution to λ_{hhh} . So, for a correct understanding of the impact on λ_{hhh} , one must take these contributions into account. In this regard, we have computed all one-loop contributions to the triple Higgs coupling using the effective potential approach as described in Ref. [24]. Note that here we are considering the limit in which the external momentum vanishes, i.e. $p^2 \rightarrow 0$, when the kinematical suppression from $p^2 \neq 0$ corrections is less or similar to the one produced by the top quark [25]. Therefore, we have considered all possible contributions coming from all physical scalars of the model (η^\pm , h_1 , h_2 , η_R , φ_R , σ_I , η_I and φ_I), as well as the loop diagram involving the virtual exchange of the top quark.

The full one-loop formulas are listed in Appendix A. In what follows, in our numerical analysis we will take into account the existing constraints on λ_{hhh} available from the LHC [26, 27]. Future collider measurements [28, 29] can further probe possible deviations of λ_{hhh} from the SM value.

Another interesting implication the considered model is the presence of potential DM candidates. First, the scalar one can be identified with the lightest among the $\text{Re } \varphi$, $\text{Im } \varphi$, $\text{Re } \eta$ and $\text{Im } \eta$ fields. Assuming for simplicity that the cosmological DM is dominated by such a scalar DM candidate, it would annihilate mainly into WW , ZZ , $t\bar{t}$, $b\bar{b}$ and $h_1 h_1$ channels in the early Universe via a Higgs portal scalar interaction. These annihilation channels will contribute to the DM relic density, which can be accommodated for appropriate values of the coupling of the Higgs portal scalar interaction and of the scalar DM mass, which in most cases are at the TeV scale. In the low mass region, namely $m_{DM} < m_h/2$, the constraints coming from the invisible Higgs decays should be taken into account. In our numerical analysis, for simplicity, these decays are kinematically forbidden. That is, we set the DM mass to be above $m_h/2$. Let us note that in the DM resonant region, i.e. $m_{DM} \sim m_h/2$, the relic density is successfully accounted for. In addition, DM direct detection implies that the scalar DM candidate would scatter off a nuclear target in a detector via Higgs boson exchange in the t -channel, giving rise to a constraint on the Higgs portal scalar interaction coupling.

The model may also feature a possible fermionic DM candidate which can be identified as the lightest among the right-handed Majorana neutrinos $N_{k,R}$ ($k = 1, 2$). Such particles are expected to annihilate into a pair of active neutrinos via t -channel exchanges of the neutral CP-even and CP-odd components of the inert scalar doublet η . The DM relic density constraints can be successfully accommodated for an appropriate region of parameter space. A detailed analysis of the implications of our model for DM studies is beyond the scope of the present work and is left for future investigations.

3 Neutrino mass and lepton flavor violation

Once Φ and σ develop VEVs, a non-trivial contribution to the neutrino mass matrix is generated at two-loop level, whose diagram is illustrated in Fig. 1. The active light neutrino mass matrix in this

case is given as,

$$(M_\nu)_{ij} = \frac{(y_N)_{in} (y_\Omega^*)_{nk} (y_\Omega^\dagger)_{kr} (y_N^T)_{rj} m_{\Psi_k}}{4(4\pi)^4} \int_0^1 d\alpha \int_0^{1-\alpha} d\beta \frac{1}{\alpha(1-\alpha)} \left[G(m_{\Psi_k}^2, m_{RR}^2, m_{RI}^2) - G(m_{\Psi_k}^2, m_{IR}^2, m_{II}^2) \right], \quad (3.1)$$

where $n, k, r = 1, 2$. Here, the loop integral I can be written as [30]

$$G(x^2, y^2, z^2) = \frac{x^2 y^2 \log\left(\frac{y^2}{x^2}\right) + y^2 z^2 \log\left(\frac{z^2}{y^2}\right) + z^2 x^2 \log\left(\frac{x^2}{z^2}\right)}{(x^2 - y^2)(x^2 - z^2)},$$

$$m_{ab}^2 = \frac{\beta m_{(\eta)_a}^2 + \alpha m_{(\varphi)_b}^2}{\alpha(1-\alpha)} \quad (a, b = R : \text{or} : I). \quad (3.2)$$

Note that the lightest active neutrino is massless which implies that there is only one Majorana phase in the PMNS matrix. A convenient way to incorporate the bounds from the neutrino oscillation data is to express the Yukawa coupling matrix using the Casas-Ibarra parametrization. For the model considered in this paper, one can express y_N as,

$$y_N = U_{\text{PMNS}}^* \sqrt{M_\nu^{\text{diag}}} R^T A^{-1}, \quad (3.3)$$

where U_{PMNS}^* is the 3×3 PMNS neutrino mixing matrix, $M_\nu^{\text{diag}} = \text{diag}(m_1, m_2, m_3)$ is the diagonal neutrino mass matrix, R is a 2×3 matrix that is given as,

$$R = \begin{pmatrix} 0 & \cos z & -\sin z \\ 0 & \sin z & \cos z \end{pmatrix} \quad \text{for normal hierarchy (NH) of light neutrino masses } (m_1 = 0) \quad \text{and}$$

$$R = \begin{pmatrix} \cos z & -\sin z & 0 \\ \sin z & \cos z & 0 \end{pmatrix} \quad \text{for inverted hierarchy (IH) of light neutrino masses } (m_3 = 0).$$

The matrix A is given by

$$A = y_\Omega^* \Lambda y_\Omega^\dagger,$$

where $\Lambda = \begin{pmatrix} \Lambda_1 & 0 \\ 0 & \Lambda_2 \end{pmatrix}$ with,

$$\Lambda_k = \frac{m_{\Psi_k}}{4(4\pi)^4} \int_0^1 d\alpha \int_0^{1-\alpha} d\beta \frac{1}{\alpha(1-\alpha)} \left[G(m_{\Psi_k}^2, m_{RR}^2, m_{RI}^2) - G(m_{\Psi_k}^2, m_{IR}^2, m_{II}^2) \right].$$

Under this parameterization, the experimentally observed neutrino mass differences and the PMNS mixing matrix can be given as input in the numerical scan, with the Yukawa coupling being found as output. Since we do not have control over the magnitude of the Yukawa couplings, we only allow solutions which respect perturbativity, i.e. $|Y_N|, |Y_\Omega| < \sqrt{4\pi}$. For the purpose of numerical scans, we only consider the normal ordering scenario for the neutrino masses (that is, $m_1 = 0$).

The presence of the Majorana fermions can induce LFV decays, such as $\mu \rightarrow e\gamma$, which are strongly constrained by experiment. In our model, such decays are mediated at one-loop level via virtual exchanges of the neutral fermions and the charged scalars. The branching fraction for the two-body decay process $\ell_i \rightarrow \ell_j \gamma$, where $i = e, \mu, \tau$ is given as [31–34]

$$\text{BR}(\ell_i \rightarrow \ell_j \gamma) = \frac{3(4\pi)^3 \alpha_{\text{em}}}{4G_F^2} \left| \frac{x_{is}^{(\nu)} x_{js}^{(\nu)}}{2(4\pi)^2 m_{\eta^\pm}^2} F\left(\frac{m_{N_{sR}}^2}{m_{\eta^\pm}^2}\right) \right|^2 \text{BR}(\ell_i \rightarrow \ell_j \nu_i \bar{\nu}_j), \quad (3.4)$$

with $s = 1, 2$. Here, $\alpha_{\text{em}} = 1/137$ is the fine-structure constant, $x_{is}^{(\nu)} = \sum_{k=1}^3 (y_N)_{ks}^{(\nu)} (V_{lL}^\dagger)_{ik}$, with V being the left-handed charged lepton mixing matrix, $G_F = 1.166364 \times 10^{-5} \text{ GeV}^{-2}$ is the Fermi constant, which in our case is the identity matrix, m_{φ^\pm} are the masses of the charged scalar components of the $\text{SU}(2)_L$ inert doublet φ , and $m_{N_{sR}}$ ($s = 1, 2$) correspond to the masses of the right-handed Majorana neutrinos N_{sR} , which due to the charge assignment, are generated at one-loop level. The loop function F is written as

$$F(x) = \frac{1 - 6x + 3x^2 + 2x^3 - 6x^2 \ln x}{6(1-x)}. \quad (3.5)$$

The most stringent bounds for LFV come from muon decay measurements, namely, $\mu \rightarrow e\gamma$. Current experimental results put an upper bound on the branching ratio, which reads as $\text{BR}(\mu \rightarrow e\gamma) < 4.2 \times 10^{-13}$ [35]. The model can also give rise to $\mu \rightarrow e$ conversion in the atomic nucleus. But the existing bounds are not as restrictive as the ones from $\text{BR}(\mu \rightarrow e\gamma)$. However, among various planned experiments, the $\mu \rightarrow e$ conversion in the Al nuclei has the best projected sensitivity of $\sim 10^{-17}$ [36]. The branching ratio for this process can approximately be expressed as [34],

$$\text{CR}(\mu \text{ Al} \rightarrow e \text{ Al}) \approx \frac{1}{350} \text{BR}(\mu \rightarrow e\gamma). \quad (3.6)$$

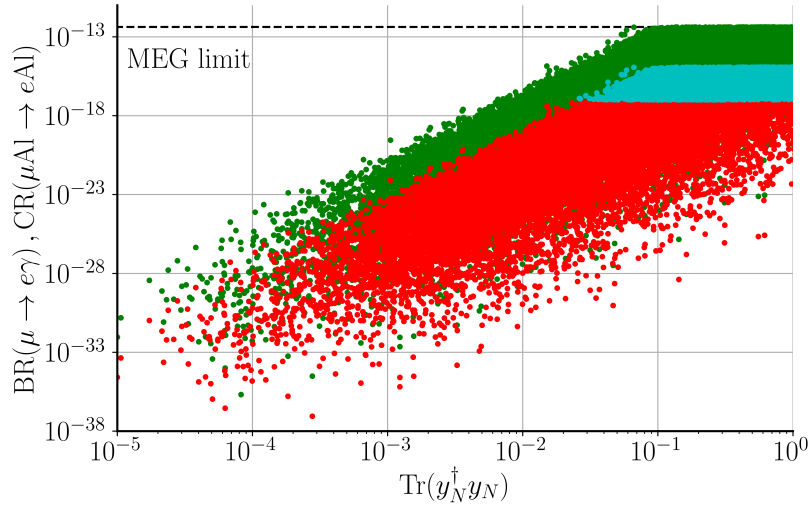


Figure 2: The predictions for $\text{BR}(\mu \rightarrow e\gamma)$ (green points) and $\text{CR}(\mu \text{ Al} \rightarrow e \text{ Al})$ (red points) as functions of $\text{Tr}[y_N^\dagger y_N]$. All the points shown are within the existing experimental bounds marked by the horizontal dashed line. The cyan points correspond to the region within the projected sensitivity for $\mu \text{ Al} \rightarrow e \text{ Al}$ conversion.

In this regards, in Fig. 2 shows the predictions for $\text{BR}(\mu \rightarrow e\gamma)$ (green points) and $\text{CR}(\mu \text{ Al} \rightarrow e \text{ Al})$ (red points) as functions of $\text{Tr}[y_N^\dagger y_N]$. Only the values that are within the existing bounds are shown, whose limit is indicated by a dashed horizontal line in the plot. The cyan points correspond to the region within the projected sensitivity for $\mu \text{ Al} \rightarrow e \text{ Al}$ conversion.

For all the points shown in Fig. 2, neutrino oscillation data is respected, with the relevant experimental parameters (namely, neutrino mass differences and the PMNS mixing angles) being given as input and allowed to vary within their respective 3σ uncertainties [37–39]. The Majorana phase is also varied in the range $[0, \pi]$ and y_Ω is taken to be diagonal where the entries are allowed to vary in the range $[0, 1]$. Here, z is defined as $x_1 + y_1 i$ with x_1 and y_1 being varied in the range $[-2, +2]$, the fermions Ψ_{kR}

and N_{kR} are taken to be degenerate, with their masses varied in the ranges $[0.5, 5]$ TeV and $[0.1, 60]$ GeV, respectively. For the scalar potential parameters, we employ the inverted equations in (2.4) to allow for the physical masses to be given as input. In this regard, we have considered the following parameter ranges:

- $m_{\eta_I}, m_{\varphi_I} \rightarrow [0.5, 3.2]$ TeV, $m_{\eta_R} \rightarrow [m_{\eta_I}, m_{\eta_I} + 5 \text{ GeV}]$, $m_{\varphi_R} \rightarrow [m_{\varphi_I}, m_{\varphi_I} + 5 \text{ GeV}]$, $m_{\eta^\pm} \rightarrow [m_{\eta_I} - 5 \text{ GeV}, m_{\eta_I}]$
- $v_1 = 246 \text{ GeV}$, $m_{h_2} \rightarrow [0.5, 5]$ TeV, $v_\sigma \rightarrow [5, 30]$ TeV,
- $\lambda_{2,5,8,9,10,11,12} \rightarrow [0, 1]$. The remaining λ 's are treated as outputs in the inversion procedure. Notice that we have inverted the expressions for λ_5 and λ_9 , which can be solved such that μ_η^2 and μ_φ^2 are instead given as output parameters, where we have taken them to be both greater than 0. Also, in the parameter space that has been considered, we have ensured that all the quartic couplings, $\lambda_i > 0$, even though this is only a sufficient condition but not necessary.

4 Phase transitions and primordial gravitational waves

One of the more interesting phenomenological consequences of extended scalar sectors compared to the SM framework is the possibility for the existence of FOPTs. Indeed, such a phenomenon is not present in the SM (both the EW and QCD phase transitions are of second order), making it pure beyond-SM driven (BSM) physics. Such transitions can lead to the generation of a SGWB. With the detection of GWs at LIGO [40], a new era of multi-messenger astronomy has arisen, where such events may give us unique perspectives into new physics beyond the SM. It has been recently proposed that the cosmological phase transitions between different vacua at finite temperatures (such as those associated with symmetry breaking in BSM models) may give rise to gravitational imprints that should be observable in future ground- and space-based experiments [41, 42]. The SGWB signals can also provide hints into the nature of the neutrino masses in the context of distinct seesaw mechanisms [43].

As the universe expands and cools down, its temperature dependent vacuum configuration evolves giving rise to transitions between different phases. If such transitions are sufficiently strongly first order, they can lead to the generation of fast expanding vacuum bubbles whose dynamics may have left a visible imprint in the form of a SGWB [44, 45]. The characteristics of the phase transition such as its strength and inverse duration depend on the underlying particle physics model described at finite temperatures and are highly sensitive, in particular, to the properties of the potential barrier between the phases and to the critical temperature of the transition (see e.g. [41, 46–50] and references therein). The phenomenon of strong FOPTs is quite generic for multi-scalar extensions of the SM (in particular, for those that undergo several symmetry breaking steps) such as the one we discuss in this article. Therefore, a SGWB from cosmological FOPTs must be regarded as an important source of phenomenological information about multi-scalar extensions of the SM which may be complementary to constraints coming from collider searches.

In order to fully classify and study the SGWB emergent in our model, there is a total of five main ingredients. The first one is inherently dependent on the considered model structure – the finite temperature effective potential [51–53]. Generically, it can be written as [54, 55]

$$V_{\text{eff}} = V^{(0)} + V_{\text{CW}}^{(1)} + V_{T \neq 0} + V_{\text{CT}}, \quad (4.1)$$

where the first term, $V^{(0)}$, is the tree-level scalar potential given in Eq. (2.2). The second term is the Coleman-Weinberg one-loop correction,

$$V_{\text{CW}}^{(1)} = \sum_a (-1)^F n_a \frac{m_a^2(\phi_b)}{64\pi^2} \left[\ln \left(\frac{m_a^2(\phi_b)}{\mu^2} \right) - C_a \right], \quad (4.2)$$

where F is 0 for bosons and 1 for fermions, $m_a(\phi_b)$ is the ϕ_a -field dependent mass of the particle a , n_a is the number of degrees of freedom for each particle a and μ is a renormalisation scale. The

particle degrees of freedom can be computed as $(-1)^{2s}QN(2s+1)$, where s is the spin of the particle, $Q = 1(2)$ for neutral (charged) particles, and N is the number of colours. In this work, we consider the $\overline{\text{MS}}$ renormalisation scheme such that we have $C_a = 3/2$ for scalars, fermions and longitudinally polarized gauge bosons, and $C_a = 1/2$ for transverse gauge bosons. Additionally, the renormalisation scale is fixed as $\mu = \prod_{i=1}^n m_{\phi_i}^{1/n}$ where i runs over all BSM scalars in the model. Since we allow to vary the masses of the scalar fields, μ will be different for each sampled point.

The third term encodes thermal corrections to the potential,

$$V_{T \neq 0} = \frac{T^4}{2\pi^2} \sum_a (-1)^F n_a J_a \left[\frac{m_a^2(\phi_a)}{T^2} \right], \quad (4.3)$$

where T is the temperature, J_0 (for bosons) and J_1 (for fermions) are the standard thermal integrals found e.g. in Ref. [54]. At the leading $(m/T)^2$ order in thermal expansions of J_a , Eq. (4.3) can be approximated as

$$\Delta V(T) \simeq \frac{T^4}{2\pi^2} \left(\text{Tr}\{M^2(\phi_\alpha)\} + \sum_{i=W,Z,\gamma} n_i m_i^2(\phi_\alpha) + \sum_{i=f_i} \frac{n_i}{2} m_i^2(\phi_\alpha) \right), \quad (4.4)$$

where in the last sum, all the fermions of the model are included. Here, M is the field-dependent Hessian matrix in the classical field approximation where all fields are fixed to their classical (background) components, that is

$$\Phi \rightarrow \begin{pmatrix} 0 \\ v_\Phi/\sqrt{2} \end{pmatrix}, \quad \sigma \rightarrow v_\sigma, \quad \eta \rightarrow \begin{pmatrix} 0 \\ 0 \end{pmatrix}, \quad \varphi \rightarrow 0, \quad (4.5)$$

and the degrees of freedom, n_i , for different states are as follows [54]: for quarks $n_a = 12$, for charged leptons $n_a = 4$, for neutral leptons $n_a = 2$, for the gauge bosons $n_W = 6$, $n_Z = 3$, $n_\gamma = 2$ and for the longitudinal component of the photon $n_{\gamma_L} = 1$. Additional higher-order corrections must also be included in the form of Daisy (ring) diagrams [51, 56–58]. These can be parameterized as thermal corrections to the quadratic mass terms of the bare potential and read as

$$\mu^2(T) \rightarrow \mu^2 + c_\phi(T^2) \equiv \mu^2 + \frac{\delta^2 \Delta V(T, \phi_a)}{\delta \phi_a}. \quad (4.6)$$

For the considered model, we have

$$\begin{aligned} c_\phi(T^2) &= \frac{T^2}{24} \left[3g^2 + \frac{3}{2}(g^2 + g_Y^2) + 12(y_b^2 + y_t^2) + 4y_\tau^2 + 12\lambda_1 + 4\lambda_5 + 2(\lambda_6 + \lambda_8 + \lambda_9) \right] \\ c_\sigma(T^2) &= \frac{T^2}{24} (4(\lambda_{10} + \lambda_8) + 2\lambda_{12} + 8\lambda_4), \end{aligned} \quad (4.7)$$

where g (g_Y) are the SU(2) (U(1)) gauge couplings and y_i are the Yukawa couplings for each of the SM-like third-generation fermions. The gauge boson masses also gain thermal corrections and, since there are no new gauge bosons in the model, the formula is identical to what is found in the previous literature (see e.g. Ref. [54]).

The last relevant part of the effective potential in Eq. (4.1) is the counter-term potential V_{CT} . The counter-terms are defined such that the minima of the tree-level potential remains fixed at zero temperature (i.e. the tree-level masses remain the same at one-loop level), which is guaranteed by imposing that the first and second derivatives of the counter-term potential match the first and second derivatives of the Coleman-Weinberg one-loop potential as

$$\left\langle \frac{\partial V_{\text{CT}}}{\partial \phi_i} \right\rangle = \left\langle -\frac{\partial V_{\text{CW}}^{(1)}}{\partial \phi_i} \right\rangle, \quad \left\langle \frac{\partial^2 V_{\text{CT}}}{\partial \phi_i \partial \phi_j} \right\rangle = \left\langle -\frac{\partial^2 V_{\text{CW}}^{(1)}}{\partial \phi_i \partial \phi_j} \right\rangle, \quad \text{with} \quad \phi_i = \{h_1, h_2\}. \quad (4.8)$$

In our case, this results in the following conditions

$$\begin{aligned}
\delta\mu_\phi &= \frac{3}{2v_\Phi} \frac{\partial V_{\text{CW}}^{(1)}}{\partial h_1} - \frac{1}{2} \frac{\partial^2 V_{\text{CW}}^{(1)}}{\partial h_1^2} + \frac{v_\sigma}{2v_\Phi} \frac{\partial^2 V_{\text{CW}}^{(1)}}{\partial h_2 \partial h_1}, & \delta\mu_{sb} &= \frac{3}{4v_\sigma} \frac{\partial V_{\text{CW}}^{(1)}}{\partial h_2} + \frac{v_\Phi}{4v_\sigma} \frac{\partial^2 V_{\text{CW}}^{(1)}}{\partial h_2 \partial h_1} - \frac{1}{4} \frac{\partial^2 V_{\text{CW}}^{(1)}}{\partial h_2^2}, \\
\delta\lambda_1 &= \frac{1}{2v_\Phi^3} \left(v_\Phi \frac{\partial^2 V_{\text{CW}}^{(1)}}{\partial h_1^2} - \frac{\partial V_{\text{CW}}^{(1)}}{\partial h_1} \right), & \delta\lambda_4 &= \frac{1}{2v_\sigma^3} \left(v_\sigma \frac{\partial^2 V_{\text{CW}}^{(1)}}{\partial h_2^2} - \frac{\partial V_{\text{CW}}^{(1)}}{\partial h_2} \right), \\
\delta\lambda_8 &= \frac{1}{v_\Phi v_\sigma} \frac{\partial V_{\text{CW}}^{(1)}}{\partial h_2 \partial h_1},
\end{aligned} \tag{4.9}$$

while for other parameters, we set $\delta\lambda_i = \delta\mu_i = 0$.

The remaining four ingredients determine the FOPT dynamics, which include [45]

- The inverse time-scale of the phase transition, β . This parameter essentially determines the bubble nucleation rate. Normalising it conventionally to the Hubble expansion rate, H , one writes

$$\frac{\beta}{H} = T_n \frac{\partial}{\partial T} \left(\frac{S(V_{\text{eff}})}{T} \right) \Big|_{T=T_n}, \tag{4.10}$$

where $S(V_{\text{eff}})$ is the Euclidean action which depends on the structure of the effective potential in Eq. (4.1).

- Nucleation temperature, T_n . It represents the temperature of the Universe directly after the phase transition, and can be computed by requiring that the probability for a single bubble nucleation per horizon volume is equal to one [59].
- Phase transition strength α , which is related to the released latent heat during the phase transition. It is found in terms of the difference between the effective potential values before and after the transition via the following relation [60, 61]

$$\alpha = \frac{30}{g_* \pi^2 T_n^2} \left[V_{\text{eff},i} - V_{\text{eff},f} - \frac{T}{4} \left(\frac{\partial V_{\text{eff},i}}{\partial T} - \frac{\partial V_{\text{eff},f}}{\partial T} \right) \right], \tag{4.11}$$

being also normalised to the radiation energy density of the Universe at the nucleation temperature. Here, g_* is the effective number of relativistic degrees of freedom in the cosmic plasma. The effective potential is evaluated at initial (metastable) phase, $V_{\text{eff},i}$, and at the final (stable) phase, $V_{\text{eff},f}$.

- Bubble wall velocity, v_b . This quantity represents the speed of the new phase at the interface of the nucleating bubble. In the current work we simply assume the case of supersonic detonations with $v_b = 0.95$. An improved analysis using the recently developed methods for the determination of the speed of sound [62] and wall velocity [63] is left for future work.

The authors are also aware of recently developed techniques accounting for a great improvement in the calculation of thermal effects, for instance, using dimensional reduction [64]. Improved studies incorporating such methods are also left for future dedicated work.

The power spectrum associated to the production of a SGWB can arise from three distinct sources,

$$h^2 \Omega_{\text{GW}} = h^2 \Omega_{\text{BC}} + h^2 \Omega_{\text{SW}} + h^2 \Omega_{\text{TURB}}. \tag{4.12}$$

Here, $h^2 \Omega_{\text{BC}}$ is the GW power spectrum produced via collision of vacuum bubbles. It offers a leading contribution when such bubbles “run-away”, that is, the friction created by the thermal plasma at the boundaries is not enough to stop the acceleration of the wall [45]. This effect is typically subleading and can usually be neglected [65], unless one is considering supercooled FOPTs [66–68]. The second term, $h^2 \Omega_{\text{SW}}$ is the power spectrum of GWs emerging from sound-waves triggered once the bubble wall sweeps through the plasma at relativistic speeds. In this case, a vast portion of the released energy

is converted to the waves' propagation in the plasma that surrounds the walls as sound waves [45]. The last term denotes the magnetohydrodynamic turbulence contribution, arising from non-linear effects of the sound waves the propagate on the plasma. The determination of such a contribution is still uncertain. Nonetheless, it is expected to be less relevant for the position of the SGWB peak amplitude and frequency in comparison to the sound waves component for supersonic detonations. Semi-analytical expressions describing each term of Eq. (4.12) with the various parameters of the FOPTs introduced above, can be found in [45, 69, 70] and references therein.

4.1 Numerical results

With a rich scalar potential, one of the immediate questions about the considered model is if it can accommodate FOPTs and if they can be strong enough to leave visible imprints in the form of a SGWB. To address this question we have implemented the thermal effective potential of the scotogenic two-loop neutrino mass model into the **CosmoTransitions** package [71] enabling us to numerically compute the bounce action and hence the probability for bubble nucleation at any given temperature. Among the key parameters that control the dynamics of the phase transitions, β/H depends on the derivative of the Euclidean effective action, and hence can exhibit numerical instabilities if the action is not numerically well-behaved. To minimize the corresponding uncertainties, we perform an interpolation of the action on a point-by-point basis. The technique for the smoothing of the Euclidean action is described in detail in some of the author's previous work [48]. Furthermore, for the scan, we have extended the ranges of various parameters to be more inclusive. Namely, we now perform a logarithmic scan over the quartic couplings in the ranges of $[10^{-8}, 4\pi]$ and the masses of the BSM scalars to be above 200 GeV. Constraints from neutrino physics and LFV observables are also imposed in the data points.

First, we show in Fig. 3 the GW peak signal, $h^2\Omega_{\text{GW}}^{\text{peak}}$, as a function of the peak frequency, f_{peak} in Hz; both axes are shown in logarithmic scale. Focusing first on the panels (a), (b) and (c) where we display in the colour axis the relevant GW observables for the dynamics of the signal, namely, the phase transition strength (a), the inverse time-scale of the phase transition (b), and the nucleation temperature (c). First, we begin by noting that various points in the parameter space can give rise to potentially detectable SGWB signals in different planned GW interferometers. The latter include the Laser Interferometer Space Antenna (LISA) [70, 72, 73], the Big Bang Observer (BBO) [74] and at the Deci-hertz Interferometer Gravitational wave Observatory (DECIGO) [75], indicating that the gravitational channel may offer a complementary approach to standard colliders channels in probing our model.

As expected, a strong correlation between the GW observables and the signal strength is found. Indeed, higher values of α imply a stronger FOPT which in turn implies lower values for both the nucleation temperature T_n and β/H . In particular, points which can be observed at LISA fall within the ranges $\alpha = [0.13, 0.88]$, $\beta/H = [81.13, 362.82]$ and $T_n = [99.77, 520.70]$ GeV. For the points within the LISA sensitivity reach, we have also computed the signal-to-noise ratio (SNR), as showcased in Fig. 4, where we note that for the strongest transitions, the corresponding SNR is greater than 200, indicating that most of these points can indeed be probed by the LISA experiment [60, 70, 76].

Now, focusing our attention on the bottom panels of Fig. 3, where we display various models parameters in the colour axis, namely, the VEV of the singlet field σ (d), the mass of the second heaviest CP-even scalar h_2 (e) and the branching ratio $\mu \rightarrow e\gamma$ (f). Here, we note that there is no strong correlation between the physical parameters of the model and the GW observables. Nevertheless, we find that for the larger values of the singlet VEV and of the mass of h_2 , while allowing for the existence of FOPTs, they give rise to higher frequency SGWB outside the sensitivity of future GW experiments. Indeed, for the parameter space regions which are accessible at LISA, the σ VEV is typically below 5 TeV whereas the h_2 mass is below 3 TeV. As for the last panel (f), we do not find any correlation with $\mu \rightarrow e\gamma$ process. Indeed, we observe that various distinct possibilities for its branching ratio can be accommodated across different values of the frequency and the signal strength.

In general, finding certain complementarity between the physical parameters of the model and SGWB observables is relevant for exploring the model's parameter space. In the context of GWs studies, it

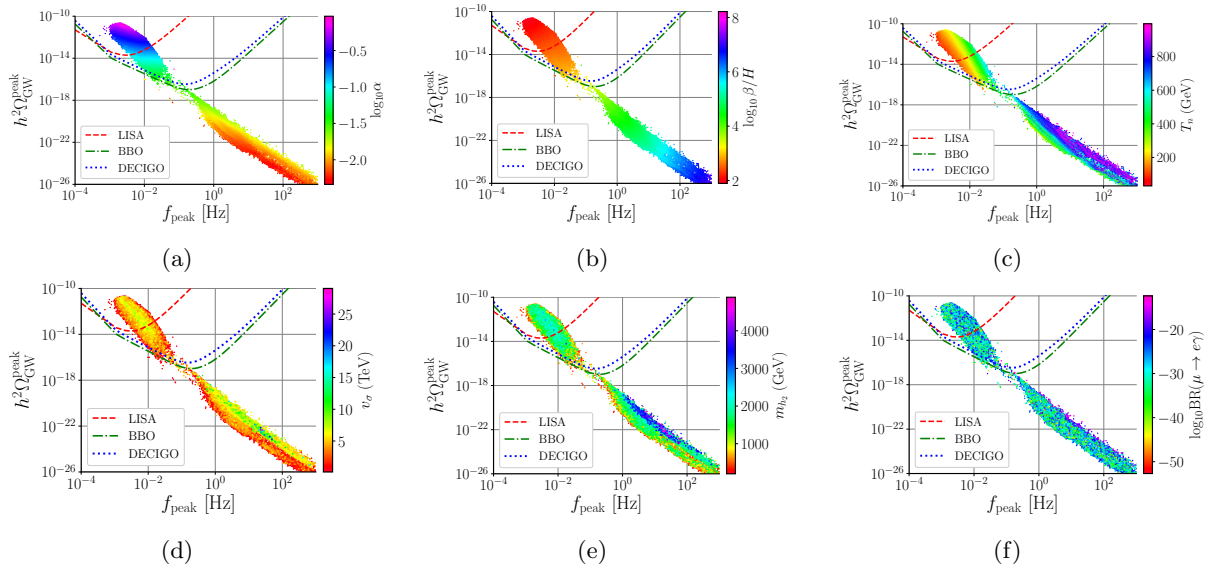


Figure 3: Peak amplitude of the GW signal, $h^2\Omega_{\text{GW}}$ as a function of the peak frequency, f_{peak} , in Hz. In colour, we have the logarithm of the phase transition strength α (a), the logarithm of the inverse time-scale of the phase transitions normalized to the Hubble parameter (b), the nucleation temperature in GeV (c), the VEV of the singlet σ field in TeV (d), the mass of the second heaviest CP-even scalar (e) and logarithm of the branching ratio of $\mu \rightarrow e\gamma$ (f). For all panels, the x -axis is displayed in logarithmic scale. All points shown here are also consistent with neutrino physics constraints as well as with constraints from the triple Higgs coupling measurements [26, 27].

has been noted in [77–80] that potentially large corrections to the trilinear Higgs coupling compared to the SM expectation can significantly affect the type and the strength of the cosmological phase transitions. Indeed, strong FOPTs can be driven by large trilinear scalar couplings as they can play a sizeable effect on the potential barrier between different vacua.

We show in Fig. 5 scatter plots for the BSM-to-SM ratio of the trilinear Higgs coupling computed for our BSM scenario versus its SM value, i.e. $\kappa \equiv \lambda_{hhh}^{\text{BSM}}/\lambda_{hhh}^{\text{SM}}$, as a function of the sine of the CP-even mixing angle, with the logarithm of the GW signal strength in colour. Here, $\lambda_{hhh}^{\text{BSM}} = \lambda_{hhh}^{\text{LO}} + \lambda_{hhh}^{\text{NLO}}$ is the full NLO result for the trilinear Higgs coupling in our model and $\lambda_{hhh}^{\text{SM}}$ corresponds to the SM prediction.

Most of the generated points satisfy $\sin\alpha_h < 0.07$. Indeed, for such low values of the scalar mixing angle, Eq. (2.5) asymptotically tends towards the SM prediction. However, NLO contributions result in a sizeable contribution to λ_{hhh} . We can also observe from panel (a) that points with larger SGWB signal tend to accumulate as one approaches the alignment limit. However, this does not represent a sufficient condition as we also find scenarios where the SGWB peak amplitude is well below the sensitivity ranges of LISA, BBO and DECIGO at low values of the scalar mixing angle, as can be readily noted in panel (b). Besides, one observes that there is a part of the parameter space that can already be excluded by the current data (gray bands) and it can be further reduced by future measurements both at the high-luminosity and high-energy phases of the LHC. However, the take home message is that even within those regions there are still several points that feature FOPTs potentially detectable at future GW facilities as a key feature of the considered model.

In Fig. 6 we show a selection of plots showing the impact of different quartic couplings and physical masses in the energy density amplitude of the GW spectra (colour axis). For panels (a), (b) and (c), we find the preferred ranges of the model’s quartic couplings that lead to observable SGWB. In particular we one obtains both $\mathcal{O}(1)$ couplings, such as e.g. λ_2 and λ_{10} and much smaller couplings such as λ_8 . Besides, we note that λ_8 is correlated with the size of the mixing for the CP-even states,

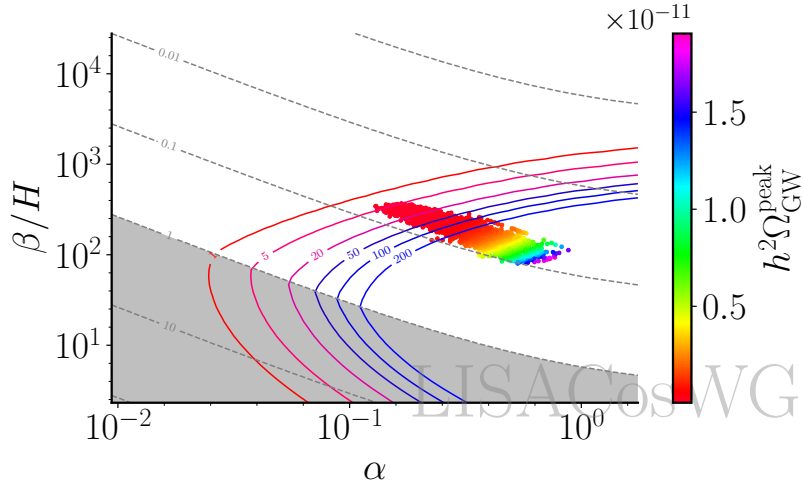


Figure 4: Signal-to-noise ratio (SNR) plot for a LISA mission profile of 3 years. In the x -axis we show the strength of the phase transition (α) and in the y -axis the inverse time duration in Hubble units. In the colour axis, we indicate the magnitude of the phase transition $h^2\Omega_{\text{GW}}^{\text{peak}}$. The coloured isolines (corresponding to the values 1, 5, 20, 50, 100 and 200) are representative of the expected values for the SNR. As a general rule of thumb, points with an SNR greater than 5 can be potentially observed. The grey area corresponds to the region where the sound-wave component is dominant. All points shown in the plot correspond to the points potentially detectable by the LISA experiment (that is, above the red LISA curves of Fig. 3).

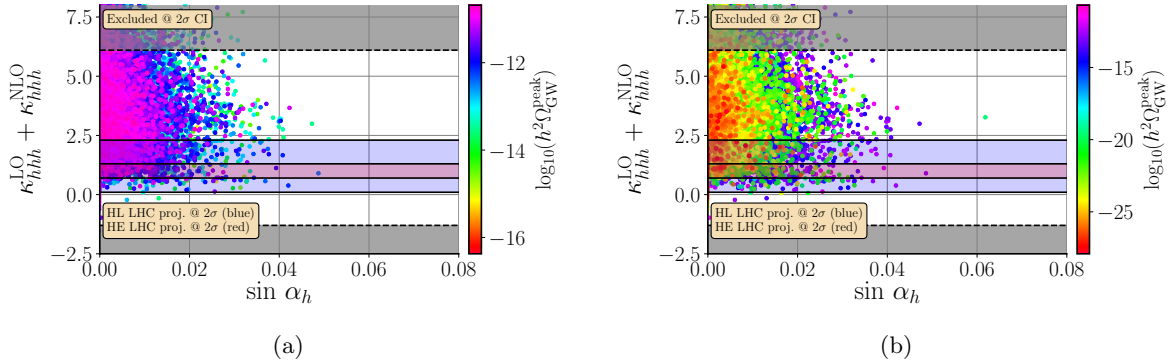


Figure 5: The BSM-to-SM ratio of trilinear Higgs couplings $\kappa \equiv \lambda_{hhh}^{\text{BSM}}/\lambda_{hhh}^{\text{SM}}$ as a function of the sine of the CP-even mixing angle α_h . On the colour axis we show the logarithm of the GW intensity. On the panel (a), the results from the full collected dataset are showcased, whereas on (b) a cut on $h^2\Omega_{\text{GW}}^{\text{peak}}$ was imposed, such that only points which are visible at future GW experiments (LISA, BBO and DECIGO) are displayed. We note that all constraints from neutrino physics and LFV are applied here. Regions marked by gray bands are excluded at 95% confidence level (CL) based on the latest results from the LHC, the blue band region corresponds to the expected sensitivity at the high-luminosity phase of the LHC [28] while the red band region corresponds to the expected sensitivity at the high-energy phase of the LHC [29].

and its smallness is related to the fact that we work very close to the alignment limit. In panels (d), (e) and (f) we notice that a wide range of physical scalar masses can be successfully accommodated with the observable GW signals. We highlight the fact that neither we did find a correlation nor

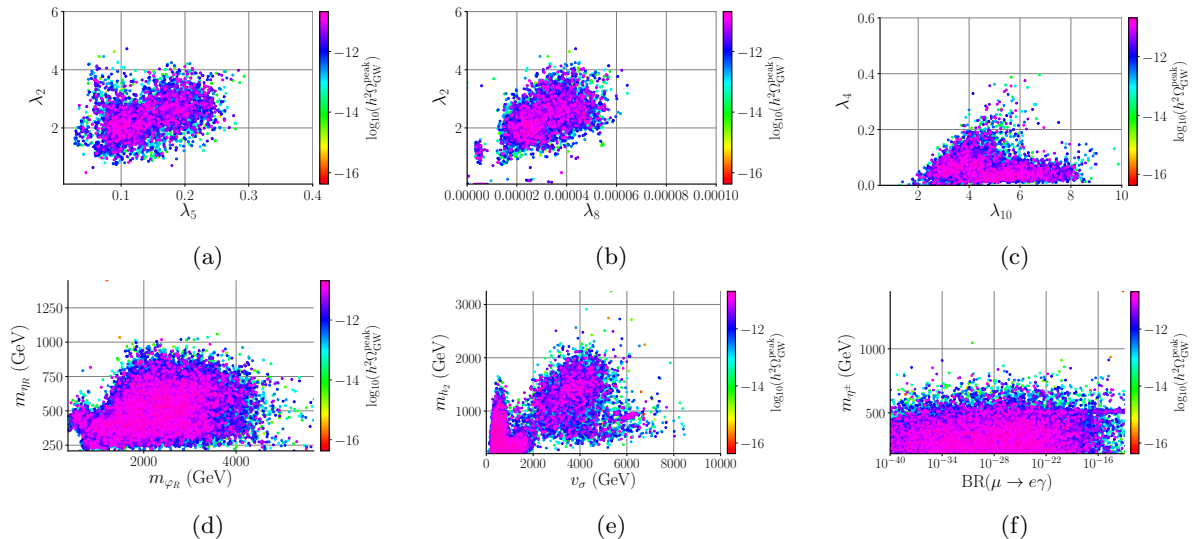


Figure 6: Scatter plots of various physical parameters of the considered model (namely, quartic couplings, physical scalar masses and VEVs) with the logarithm of the GW intensity shown in the colour axis. In particular, we show λ_2 as a function of λ_5 (a), λ_2 as a function of λ_8 (b), λ_4 as a function of λ_{10} (c), the mass of η_R as a function of the φ_R mass (d), the h_2 mass as a function of the singlet σ VEV (e), and the mass of the charged scalar η^\pm as a function of the branching ratio of $\mu \rightarrow e\gamma$ decay. The masses are given in units of GeV. Here, a cut on $h^2\Omega_{\text{peak}}^{\text{GW}}$ was imposed, such that only points which are visible at future GW experiments (either at LISA, BBO or DECIGO) are displayed. In panel (f), the x -axis is shown in logarithmic scale.

additional restrictions on the quartic couplings λ_7 and λ_{13} involved in the neutrino mass generation. These parameters can take either small or large values without modifying the conclusions of this section. It can also be noted that no apparent correlation between the $\mu \rightarrow e\gamma$ decay rate and the mass of the charged scalar field is present, exhibiting a distinct flat distribution where most of the charged scalar masses tend to be below 1 TeV.

5 Conclusions

In this work, we have presented a new scotogenic two-loop neutrino mass model where the SM gauge group is extended with an additional global $U(1) \times Z_2$ symmetry. The scalar sector of this framework contains the standard Higgs doublet, inert scalar doublet, singlet scalar fields as well as an active scalar singlet. Additionally, the model features the sector of right-handed Majorana neutrinos which in combination with the new exotic scalars leads to the generation of neutrino mass and mixing at two-loop level. The presence of Majorana neutrinos, together with a physical charged scalar field, also generates highly suppressed contributions to the tightly constrained LFV observables.

The presence of a rich scalar sector in this model opens up the possibility for testing it at both collider and GW experiments. In particular, our model features the generation of cosmological FOPTs in the early Universe that can lead to the formation of potentially observable SGWB. Focusing primarily on the phenomenologically favourable Higgs alignment limit, where the mixing between the CP-even states is small, we have performed a parameter scan of the model taking into account relevant constraints from LFV processes (such as $\mu \rightarrow e\gamma$ decay) and those from neutrino physics. In this article we have identified which regions of the parameter space can successfully accommodate the existing constraints and giving rise to strong FOPTs that lead to an observable SGWB at LISA. In addition, we have taken into account the constraints on the trilinear Higgs coupling at the NLO, and

found a number of points with visible SGWB that can be probed in both collider and GW experiments in a foreseeable future.

Acknowledgments

This work was supported by the grants CERN/FIS-PAR/0021/2021, CERN/FIS-PAR/0019/2021, CERN/FIS-PAR/0024/2021, CERN/FIS-PAR/0025/2021 and PTDC/FIS-AST/3041/2020. A.E.C.H. acknowledges support by FONDECYT (Chile) under grant No. 1210378, Milenio-ANID-ICN2019_044 and ANID PIA/APOYO AFB220004. The work of C.B. was supported by FONDECYT grant No. 11201240. V.K.N. is supported by ANID-Chile Fondecyt Postdoctoral grant No. 3220005. R.P. is supported in part by the Swedish Research Council grant, contract number 2016-05996, as well as by the European Research Council (ERC) under the European Union’s Horizon 2020 research and innovation programme (grant agreement No 668679). A.P.M. and J.G. are supported by the Center for Research and Development in Mathematics and Applications (CIDMA) through the Portuguese Foundation for Science and Technology (FCT - Fundação para a Ciência e a Tecnologia), references UIDB/04106/2020 and UIDP/04106/2020. A.P.M. is also supported by national funds (OE), through FCT, I.P., in the scope of the framework contract foreseen in the numbers 4, 5 and 6 of the article 23, of the Decree-Law 57/2016, of August 29, changed by Law 57/2017, of July 19. J.G. is also directly funded by FCT through the doctoral program grant with the reference 2021.04527.BD. The authors also would like to acknowledge the FCT Advanced Computing Project to provide computational resources via the project CPCA/A00/7395/2020. This work was partially produced with the support of INCID funded by FCT and FEDER under the project 01/SAICT/2016 n^o 022153. C.B. would like to acknowledge the hospitality and support from the ICTP through the Associates Programme (2023-2028).

A One-loop expression for the physical trilinear Higgs coupling

In the zero external momentum approximation, only fields with the mass near or above the Higgs field provide with leading corrections to the Higgs triple coupling, which in our model includes the top quark and all BSM scalar fields at the NLO. The neutral heavy Majorana fields do not contribute to the amplitude, since they do not couple directly to the Higgs boson before and after the EW symmetry breaking. Following Ref. [24], the one-loop corrections involving the top quark reads as

$$\lambda_{hhh}^t = \frac{1}{32\pi^2} \left[-36(\mathcal{F}(m_t, m_t) - 1)\lambda_{tth}^{(0)}\lambda_{tthh}^{(0)} - 24\mathcal{F}(m_t, m_t, m_t)(\lambda_{tth}^{(0)})^3 \right], \quad (\text{A.1})$$

where m_t 172.76 GeV is the top mass. The NLO contribution coming from the scalar fields reads

$$\begin{aligned} \lambda_{hhh}^\phi = \frac{1}{32\pi^2} & \left[4\mathcal{F}(m_{\eta^\pm}, m_{\eta^\pm}, m_{\eta^\pm})(\lambda_{h_1\eta^\pm\eta^\pm}^{(0)})^3 + 2\sum_{k=2}^8 \mathcal{F}(m_k, m_k, m_k)(\lambda_{h_1kk}^{(0)})^3 + \right. \\ & 6\mathcal{F}(m_{h_2}, m_{h_2}, m_{h_1})(\lambda_{h_1,h_1,h_2}^{(0)})^2 \sum_{k=2}^3 \lambda_{h_1kk}^{(0)} + 2\mathcal{F}(m_{\eta_R}, m_{\eta_R}, m_{\eta_R})(\lambda_{h_1\eta_R\eta_R}^{(0)})^3 - \\ & 3\sum_{k=2}^8 (\mathcal{F}(m_k, m_k) - 1)\lambda_{h_1kk}^{(0)}\lambda_{h_1h_1kk}^{(0)} + 6(\mathcal{F}(m_{\eta^\pm}, m_{\eta^\pm}) - 1)\lambda_{h_1\eta^\pm\eta^\pm}^{(0)}\lambda_{h_1h_1\eta^\pm\eta^\pm}^{(0)} + \\ & \left. 6(\mathcal{F}(m_{h_1}, m_{h_2}) - 1)\lambda_{h_1h_1h_2}^{(0)}\lambda_{h_1h_1h_2h_2}^{(0)} \right], \quad (\text{A.2}) \end{aligned}$$

where for simplicity of presentation we have $k = 1 \dots 8 \equiv \eta^\pm, h_1, h_2, \eta_R, \varphi_R, \sigma_I, \eta_I, \varphi_I$. The superscript “(0)” indicates tree-level accuracy. The loop function \mathcal{F} is defined as [24]

$$\mathcal{F}(m_{a_1} \dots m_{a_N}) = \sum_{x=1}^N \frac{m_{a_x}^2 \log\left(\frac{m_{a_x}^2}{\mu^2}\right)}{\prod_{y \neq x} (m_{a_x}^2 - m_{a_y}^2)}, \quad (\text{A.3})$$

where μ is the renormalisation scale. Here, we have used the same definition for the scale as in the calculation of the Coleman-Weinberg potential, i.e. the renormalisation scale is defined as $\mu = \prod_{i=1}^n m_{\phi_i}^{1/n}$, where i runs over all BSM scalars in the model. The various λ couplings in the previous expressions are written as

$$\lambda_{tth}^{(0)} = 4 \cos(\alpha_h) y_t^2 v, \quad (\text{A.4})$$

$$\lambda_{ttth}^{(0)} = 4 \cos^2(\alpha_h) y_t^2, \quad (\text{A.5})$$

$$\lambda_{h_1 \eta^\pm \eta^\pm}^{(0)} = \sin(\alpha_h) \lambda_{10} v_\sigma + \cos(\alpha_h) \lambda_5 v, \quad (\text{A.6})$$

$$\lambda_{h_1 h_1 h_1}^{(0)} = 6 \cos^3(\alpha_h) v \lambda_1 + 6 \sin^3(\alpha_h) v_\sigma \lambda_4 + 3 \cos(\alpha_h) \sin^2(\alpha_h) v \lambda_8 + 3 \cos^2(\alpha_h) \sin(\alpha_h) v_\sigma \lambda_8, \quad (\text{A.7})$$

$$\lambda_{h_1 h_2 h_2}^{(0)} = 6 \lambda_1 v \sin^2(\alpha_h) \cos(\alpha_h) + \lambda_8 v \cos^3(\alpha_h) - 2 \lambda_8 v \sin^2(\alpha_h) \cos(\alpha_h) - 6 \lambda_4 v_\sigma \sin(\alpha_h) \cos^2(\alpha_h) - \lambda_8 v_\sigma \sin^3(\alpha_h) + 2 \lambda_8 \sin(\alpha_h) \cos^2(\alpha_h), \quad (\text{A.8})$$

$$\lambda_{h_1 \eta_R \eta_R}^{(0)} = v \cos(\alpha_h) (\lambda_5 + \lambda_7) - \lambda_{10} v_\sigma \sin(\alpha_h), \quad (\text{A.9})$$

$$\lambda_{h_1 \varphi_R \varphi_R}^{(0)} = \lambda_9 v \cos(\alpha_h) - v_\sigma \sin(\alpha_h) (\lambda_{12} + \lambda_{13}), \quad (\text{A.10})$$

$$\lambda_{h_1 \sigma_I \sigma_I}^{(0)} = \lambda_8 v_1 \cos(\alpha_h) - 2 \lambda_4 v_\sigma \sin(\alpha_h), \quad (\text{A.11})$$

$$\lambda_{h_1 \eta_I \eta_I}^{(0)} = v_1 \cos(\alpha_h) (\lambda_5 - \lambda_7) - \lambda_{10} v_\sigma \sin(\alpha_h), \quad (\text{A.12})$$

$$\lambda_{h_1 \varphi_I \varphi_I}^{(0)} = \lambda_9 v_1 \cos(\alpha_h) - v_\sigma \sin(\alpha_h) (\lambda_{12} - \lambda_{13}), \quad (\text{A.13})$$

$$\lambda_{h_1 h_1 h_2}^{(0)} = 6 \lambda_1 v \sin(\alpha_h) \cos^2(\alpha_h) + \lambda_8 v \sin^3(\alpha_h) - 2 \lambda_8 v \sin(\alpha_h) \cos^2(\alpha_h) + 6 \lambda_4 v_\sigma \sin^2(\alpha_h) \cos(\alpha_h) + \lambda_8 v_\sigma \cos^3(\alpha_h) - 2 \lambda_8 v_\sigma \sin^2(\alpha_h) \cos(\alpha_h), \quad (\text{A.14})$$

$$\lambda_{h_1 h_1 \eta^\pm \eta^\pm}^{(0)} = \lambda_{10} \sin^2(\alpha_h) + \lambda_5 \cos^2(\alpha_h), \quad (\text{A.15})$$

$$\lambda_{h_1 h_1 h_1 h_1}^{(0)} = 6 \lambda_1 \cos^4(\alpha_h) + 6 \lambda_4 \sin^4(\alpha_h) + 6 \lambda_8 \sin^2(\alpha_h) \cos^2(\alpha_h), \quad (\text{A.16})$$

$$\lambda_{h_1 h_1 h_2 h_2}^{(0)} = 6 \lambda_1 \sin^2(\alpha_h) \cos^2(\alpha_h) + 6 \lambda_4 \sin^2(\alpha_h) \cos^2(\alpha_h) + \lambda_8 \sin^4(\alpha_h) + \lambda_8 \cos^4(\alpha_h) - 4 \lambda_8 \sin^2(\alpha_h) \cos^2(\alpha_h), \quad (\text{A.17})$$

$$\lambda_{h_1 h_1 h_2 h_2}^{(0)} = 6 \lambda_1 \sin^2(\alpha_h) \cos^2(\alpha_h) + 6 \lambda_4 \sin^2(\alpha_h) \cos^2(\alpha_h) + \lambda_8 \sin^4(\alpha_h) + \lambda_8 \cos^4(\alpha_h) - 4 \lambda_8 \sin^2(\alpha_h) \cos^2(\alpha_h), \quad (\text{A.18})$$

$$\lambda_{h_1 h_1 \eta_R \eta_R}^{(0)} = \lambda_{10} \sin^2(\alpha_h) + \cos^2(\alpha_h) (\lambda_5 + \lambda_7), \quad (\text{A.19})$$

$$\lambda_{h_1 h_1 \varphi_R \varphi_R}^{(0)} = \sin^2(\alpha_h) (\lambda_{12} + \lambda_{13}) + \lambda_9 \cos^2(\alpha_h), \quad (\text{A.20})$$

$$\lambda_{h_1 h_1 \sigma_I \sigma_I}^{(0)} = 2 \lambda_4 \sin^2(\alpha_h) + \lambda_8 \cos^2(\alpha_h), \quad (\text{A.21})$$

$$\lambda_{h_1 h_1 \eta_I \eta_I}^{(0)} = \lambda_{10} \sin^2(\alpha_h) + \cos^2(\alpha_h) (\lambda_5 - \lambda_7), \quad (\text{A.22})$$

$$\lambda_{h_1 h_1 \varphi_I \varphi_I}^{(0)} = \sin^2(\alpha_h) (\lambda_{12} - \lambda_{13}) + \lambda_9 \cos^2(\alpha_h), \quad (\text{A.23})$$

such that the trilinear Higgs coupling at one-loop accuracy is determined as $\lambda_{hhh}^{\text{NLO}} = \lambda_{h_1 h_1 h_1}^{(0)} + \lambda_{hhh}^t + \lambda_{hhh}^\phi$.

References

- [1] Y. Cai, J. Herrero-García, M. A. Schmidt, A. Vicente, and R. R. Volkas, *From the trees to the forest: a review of radiative neutrino mass models*, *Front. in Phys.* **5** (2017) 63, [[1706.08524](#)].
- [2] P. Minkowski, $\mu \rightarrow e\gamma$ at a Rate of One Out of 10^9 Muon Decays?, *Phys. Lett. B* **67** (1977) 421–428.
- [3] T. Yanagida, *Horizontal gauge symmetry and masses of neutrinos*, *Conf. Proc. C* **7902131** (1979) 95–99.
- [4] S. L. Glashow, *The Future of Elementary Particle Physics*, *NATO Sci. Ser. B* **61** (1980) 687.
- [5] R. N. Mohapatra and G. Senjanovic, *Neutrino Mass and Spontaneous Parity Nonconservation*, *Phys. Rev. Lett.* **44** (1980) 912.

- [6] M. Gell-Mann, P. Ramond, and R. Slansky, *Complex Spinors and Unified Theories*, *Conf. Proc. C* **790927** (1979) 315–321, [[1306.4669](#)].
- [7] J. Schechter and J. W. F. Valle, *Neutrino Masses in $SU(2) \times U(1)$ Theories*, *Phys. Rev. D* **22** (1980) 2227.
- [8] J. Schechter and J. W. F. Valle, *Neutrino Decay and Spontaneous Violation of Lepton Number*, *Phys. Rev. D* **25** (1982) 774.
- [9] C. Bonilla, E. Ma, E. Peinado, and J. W. F. Valle, *Two-loop Dirac neutrino mass and WIMP dark matter*, *Phys. Lett. B* **762** (2016) 214–218, [[1607.03931](#)].
- [10] S. Baek, H. Okada, and Y. Orikasa, *A Two Loop Radiative Neutrino Model*, *Nucl. Phys. B* **941** (2019) 744–754, [[1703.00685](#)].
- [11] S. Saad, *Origin of a two-loop neutrino mass from $SU(5)$ grand unification*, *Phys. Rev. D* **99** (2019), no. 11 115016, [[1902.11254](#)].
- [12] T. Nomura and H. Okada, *A two loop induced neutrino mass model with modular A_4 symmetry*, *Nucl. Phys. B* **966** (2021) 115372, [[1906.03927](#)].
- [13] C. Arbeláez, A. E. Cárcamo Hernández, R. Cepedello, M. Hirsch, and S. Kovalenko, *Radiative type-I seesaw neutrino masses*, *Phys. Rev. D* **100** (2019), no. 11 115021, [[1910.04178](#)].
- [14] S. Saad, *Combined explanations of $(g - 2)_\mu$, $R_{D^{(*)}}$, $R_{K^{(*)}}$ anomalies in a two-loop radiative neutrino mass model*, *Phys. Rev. D* **102** (2020), no. 1 015019, [[2005.04352](#)].
- [15] Z.-z. Xing and D. Zhang, *On the two-loop radiative origin of the smallest neutrino mass and the associated Majorana CP phase*, *Phys. Lett. B* **807** (2020) 135598, [[2005.05171](#)].
- [16] C.-H. Chen and T. Nomura, *Two-loop radiative seesaw, muon $g - 2$, and τ -lepton-flavor violation with DM constraints*, *JHEP* **09** (2021) 090, [[2001.07515](#)].
- [17] T. Nomura, H. Okada, and Y. Uesaka, *A two-loop induced neutrino mass model, dark matter, and LFV processes $\ell_i \rightarrow \ell_j \gamma$, and $\mu e \rightarrow ee$ in a hidden local $U(1)$ symmetry*, *Nucl. Phys. B* **962** (2021) 115236, [[2008.02673](#)].
- [18] S. Jana, P. K. Vishnu, and S. Saad, *Minimal realizations of Dirac neutrino mass from generic one-loop and two-loop topologies at $d = 5$* , *JCAP* **04** (2020) 018, [[1910.09537](#)].
- [19] C. Arbeláez, R. Cepedello, J. C. Helo, M. Hirsch, and S. Kovalenko, *How many 1-loop neutrino mass models are there?*, *JHEP* **08** (2022) 023, [[2205.13063](#)].
- [20] C. Bonilla, S. Centelles-Chuliá, R. Cepedello, E. Peinado, and R. Srivastava, *Dark matter stability and Dirac neutrinos using only Standard Model symmetries*, *Phys. Rev. D* **101** (2020), no. 3 033011, [[1812.01599](#)].
- [21] P. Basler, M. Mühlleitner, and J. Müller, *Electroweak Phase Transition in Non-Minimal Higgs Sectors*, *JHEP* **05** (2020) 016, [[1912.10477](#)].
- [22] H. Bahl, J. Braathen, and G. Weiglein, *New Constraints on Extended Higgs Sectors from the Trilinear Higgs Coupling*, *Phys. Rev. Lett.* **129** (2022), no. 23 231802, [[2202.03453](#)].
- [23] P. Osland, P. N. Pandita, and L. Selbuz, *Trilinear Higgs couplings in the two Higgs doublet model with CP violation*, *Phys. Rev. D* **78** (2008) 015003, [[0802.0060](#)].
- [24] J. E. Camargo-Molina, A. P. Morais, R. Pasechnik, M. O. P. Sampaio, and J. Wessén, *All one-loop scalar vertices in the effective potential approach*, *JHEP* **08** (2016) 073, [[1606.07069](#)].
- [25] J. R. Ellis, G. Ridolfi, and F. Zwirner, *Radiative corrections to the masses of supersymmetric Higgs bosons*, *Phys. Lett. B* **257** (1991) 83–91.
- [26] **ATLAS** Collaboration, *Constraining the Higgs boson self-coupling from single- and double-Higgs production with the ATLAS detector using pp collisions at $\sqrt{s} = 13$ TeV*, tech. rep., CERN, Geneva, 2022. All figures including auxiliary figures are available at <https://atlas.web.cern.ch/Atlas/GROUPS/PHYSICS/CONFNOTES/ATLAS-CONF-2022-050>.
- [27] **ATLAS** Collaboration, *Combination of searches for non-resonant and resonant Higgs boson pair production in the $b\bar{b}\gamma\gamma$, $b\bar{b}\tau^+\tau^-$ and $b\bar{b}b\bar{b}$ decay channels using pp collisions at $\sqrt{s} = 13$ TeV with the*

ATLAS detector, tech. rep., CERN, Geneva, 2021. All figures including auxiliary figures are available at <https://atlas.web.cern.ch/Atlas/GROUPS/PHYSICS/CONFNOTES/ATLAS-CONF-2021-052>.

- [28] **ATLAS** Collaboration, *Snowmass White Paper Contribution: Physics with the Phase-2 ATLAS and CMS Detectors*, tech. rep., CERN, Geneva, 2022. All figures including auxiliary figures are available at <https://atlas.web.cern.ch/Atlas/GROUPS/PHYSICS/PUBNOTES/ATL-PHYS-PUB-2022-018>.
- [29] S. Homiller and P. Meade, *Measurement of the Triple Higgs Coupling at a HE-LHC*, *JHEP* **03** (2019) 055, [[1811.02572](#)].
- [30] Y. Kajiyama, H. Okada, and T. Toma, *Multicomponent dark matter particles in a two-loop neutrino model*, *Phys. Rev. D* **88** (2013), no. 1 015029, [[1303.7356](#)].
- [31] E. Ma and M. Raidal, *Neutrino mass, muon anomalous magnetic moment, and lepton flavor nonconservation*, *Phys. Rev. Lett.* **87** (2001) 011802, [[hep-ph/0102255](#)]. [Erratum: *Phys.Rev.Lett.* **87**, 159901 (2001)].
- [32] T. Toma and A. Vicente, *Lepton Flavor Violation in the Scotogenic Model*, *JHEP* **01** (2014) 160, [[1312.2840](#)].
- [33] A. Vicente and C. E. Yaguna, *Probing the scotogenic model with lepton flavor violating processes*, *JHEP* **02** (2015) 144, [[1412.2545](#)].
- [34] M. Lindner, M. Platscher, and F. S. Queiroz, *A Call for New Physics : The Muon Anomalous Magnetic Moment and Lepton Flavor Violation*, *Phys. Rept.* **731** (2018) 1–82, [[1610.06587](#)].
- [35] **MEG** Collaboration, A. M. Baldini *et al.*, *Search for the lepton flavour violating decay $\mu^+ \rightarrow e^+ \gamma$ with the full dataset of the MEG experiment*, *Eur. Phys. J. C* **76** (2016), no. 8 434, [[1605.05081](#)].
- [36] R. H. Bernstein and P. S. Cooper, *Charged Lepton Flavor Violation: An Experimenter’s Guide*, *Phys. Rept.* **532** (2013) 27–64, [[1307.5787](#)].
- [37] F. Capozzi, E. Di Valentino, E. Lisi, A. Marrone, A. Melchiorri, and A. Palazzo, *Global constraints on absolute neutrino masses and their ordering*, *Phys. Rev. D* **95** (2017), no. 9 096014, [[2003.08511](#)]. [Addendum: *Phys.Rev.D* 101, 116013 (2020)].
- [38] I. Esteban, M. C. Gonzalez-Garcia, M. Maltoni, T. Schwetz, and A. Zhou, *The fate of hints: updated global analysis of three-flavor neutrino oscillations*, *JHEP* **09** (2020) 178, [[2007.14792](#)].
- [39] P. F. de Salas, D. V. Forero, S. Gariazzo, P. Martínez-Miravé, O. Mena, C. A. Ternes, M. Tórtola, and J. W. F. Valle, *2020 global reassessment of the neutrino oscillation picture*, *JHEP* **02** (2021) 071, [[2006.11237](#)].
- [40] **LIGO Scientific, Virgo** Collaboration, B. P. Abbott *et al.*, *Observation of Gravitational Waves from a Binary Black Hole Merger*, *Phys. Rev. Lett.* **116** (2016), no. 6 061102, [[1602.03837](#)].
- [41] A. Greljo, T. Opferkuch, and B. A. Stefanek, *Gravitational Imprints of Flavor Hierarchies*, *Phys. Rev. Lett.* **124** (2020), no. 17 171802, [[1910.02014](#)].
- [42] S. F. King, S. Pascoli, J. Turner, and Y.-L. Zhou, *Gravitational Waves and Proton Decay: Complementary Windows into Grand Unified Theories*, *Phys. Rev. Lett.* **126** (2021), no. 2 021802, [[2005.13549](#)].
- [43] A. Addazi, A. Marcianò, A. P. Morais, R. Pasechnik, R. Srivastava, and J. W. F. Valle, *Gravitational footprints of massive neutrinos and lepton number breaking*, *Phys. Lett. B* **807** (2020) 135577, [[1909.09740](#)].
- [44] A. Kosowsky and M. S. Turner, *Gravitational radiation from colliding vacuum bubbles: envelope approximation to many bubble collisions*, *Phys. Rev. D* **47** (1993) 4372–4391, [[astro-ph/9211004](#)].
- [45] K. Hashino, R. Jinno, M. Kakizaki, S. Kanemura, T. Takahashi, and M. Takimoto, *Selecting models of first-order phase transitions using the synergy between collider and gravitational-wave experiments*, *Phys. Rev. D* **99** (2019), no. 7 075011, [[1809.04994](#)].
- [46] A. P. Morais and R. Pasechnik, *Probing multi-step electroweak phase transition with multi-peaked primordial gravitational waves spectra*, *JCAP* **04** (2020) 036, [[1910.00717](#)].

- [47] J. M. Cline, A. Friedlander, D.-M. He, K. Kainulainen, B. Laurent, and D. Tucker-Smith, *Baryogenesis and gravity waves from a UV-completed electroweak phase transition*, *Phys. Rev. D* **103** (2021), no. 12 123529, [[2102.12490](#)].
- [48] F. F. Freitas, G. Lourenço, A. P. Morais, A. Nunes, J. a. Olívia, R. Pasechnik, R. Santos, and J. a. Viana, *Impact of SM parameters and of the vacua of the Higgs potential in gravitational waves detection*, *JCAP* **03** (2022), no. 03 046, [[2108.12810](#)].
- [49] Z. Zhang, C. Cai, X.-M. Jiang, Y.-L. Tang, Z.-H. Yu, and H.-H. Zhang, *Phase transition gravitational waves from pseudo-Nambu-Goldstone dark matter and two Higgs doublets*, *JHEP* **05** (2021) 160, [[2102.01588](#)].
- [50] P. Di Bari, D. Marfatia, and Y.-L. Zhou, *Gravitational waves from first-order phase transitions in Majoron models of neutrino mass*, *JHEP* **10** (2021) 193, [[2106.00025](#)].
- [51] L. Dolan and R. Jackiw, *Symmetry Behavior at Finite Temperature*, *Phys. Rev. D* **9** (1974) 3320–3341.
- [52] S. Weinberg, *Gauge and Global Symmetries at High Temperature*, *Phys. Rev. D* **9** (1974) 3357–3378.
- [53] R. H. Brandenberger, *Quantum Field Theory Methods and Inflationary Universe Models*, *Rev. Mod. Phys.* **57** (1985) 1.
- [54] M. Quiros, *Finite temperature field theory and phase transitions*, in *ICTP Summer School in High-Energy Physics and Cosmology*, pp. 187–259, 1, 1999. [hep-ph/9901312](#).
- [55] D. Curtin, P. Meade, and H. Ramani, *Thermal Resummation and Phase Transitions*, *Eur. Phys. J. C* **78** (2018), no. 9 787, [[1612.00466](#)].
- [56] R. R. Parwani, *Resummation in a hot scalar field theory*, *Phys. Rev. D* **45** (1992) 4695, [[hep-ph/9204216](#)]. [Erratum: *Phys.Rev.D* 48, 5965 (1993)].
- [57] P. B. Arnold and O. Espinosa, *The Effective potential and first order phase transitions: Beyond leading-order*, *Phys. Rev. D* **47** (1993) 3546, [[hep-ph/9212235](#)]. [Erratum: *Phys.Rev.D* 50, 6662 (1994)].
- [58] J. R. Espinosa and M. Quiros, *Improved metastability bounds on the standard model Higgs mass*, *Phys. Lett. B* **353** (1995) 257–266, [[hep-ph/9504241](#)].
- [59] J. M. Moreno, M. Quiros, and M. Seco, *Bubbles in the supersymmetric standard model*, *Nucl. Phys. B* **526** (1998) 489–500, [[hep-ph/9801272](#)].
- [60] M. Hindmarsh, S. J. Huber, K. Rummukainen, and D. J. Weir, *Shape of the acoustic gravitational wave power spectrum from a first order phase transition*, *Phys. Rev. D* **96** (2017), no. 10 103520, [[1704.05871](#)]. [Erratum: *Phys.Rev.D* 101, 089902 (2020)].
- [61] M. Hindmarsh, S. J. Huber, K. Rummukainen, and D. J. Weir, *Numerical simulations of acoustically generated gravitational waves at a first order phase transition*, *Phys. Rev. D* **92** (2015), no. 12 123009, [[1504.03291](#)].
- [62] T. V. I. Tenkanen and J. van de Vis, *Speed of sound in cosmological phase transitions and effect on gravitational waves*, *JHEP* **08** (2022) 302, [[2206.01130](#)].
- [63] W.-Y. Ai, B. Laurent, and J. van de Vis, *Model-independent bubble wall velocities in local thermal equilibrium*, [2303.10171](#).
- [64] A. Ekstedt, P. Schicho, and T. V. I. Tenkanen, *DRalgo: a package for effective field theory approach for thermal phase transitions*, [2205.08815](#).
- [65] D. Bodeker and G. D. Moore, *Electroweak Bubble Wall Speed Limit*, *JCAP* **05** (2017) 025, [[1703.08215](#)].
- [66] M. Kierkla, A. Karam, and B. Swieżewska, *Conformal model for gravitational waves and dark matter: a status update*, *JHEP* **03** (2023) 007, [[2210.07075](#)].
- [67] T. Prokopec, J. Rezacek, and B. Świeżewska, *Gravitational waves from conformal symmetry breaking*, *JCAP* **02** (2019) 009, [[1809.11129](#)].
- [68] J. Ellis, M. Lewicki, and V. Vaskonen, *Updated predictions for gravitational waves produced in a strongly supercooled phase transition*, *JCAP* **11** (2020) 020, [[2007.15586](#)].
- [69] **LISA Cosmology Working Group** Collaboration, P. Auclair *et al.*, *Cosmology with the Laser Interferometer Space Antenna*, [2204.05434](#).

- [70] C. Caprini *et al.*, *Detecting gravitational waves from cosmological phase transitions with LISA: an update*, *JCAP* **03** (2020) 024, [[1910.13125](#)].
- [71] C. L. Wainwright, *CosmoTransitions: Computing Cosmological Phase Transition Temperatures and Bubble Profiles with Multiple Fields*, *Comput. Phys. Commun.* **183** (2012) 2006–2013, [[1109.4189](#)].
- [72] P. Amaro-Seoane *et al.*, *Laser Interferometer Space Antenna*, [1702.00786](#).
- [73] C. Caprini *et al.*, *Science with the space-based interferometer eLISA. II: Gravitational waves from cosmological phase transitions*, *JCAP* **04** (2016) 001, [[1512.06239](#)].
- [74] V. Corbin and N. J. Cornish, *Detecting the cosmic gravitational wave background with the big bang observer*, *Class. Quant. Grav.* **23** (2006) 2435–2446, [[gr-qc/0512039](#)].
- [75] H. Kudoh, A. Taruya, T. Hiramatsu, and Y. Himemoto, *Detecting a gravitational-wave background with next-generation space interferometers*, *Phys. Rev. D* **73** (2006) 064006, [[gr-qc/0511145](#)].
- [76] D. J. Weir, *PTPlot: a tool for exploring the gravitational wave power spectrum from first-order phase transitions*, Aug., 2022.
- [77] R. Zhou, W. Cheng, X. Deng, L. Bian, and Y. Wu, *Electroweak phase transition and Higgs phenomenology in the Georgi-Machacek model*, *JHEP* **01** (2019) 216, [[1812.06217](#)].
- [78] A. Ahriche, K. Hashino, S. Kanemura, and S. Nasri, *Gravitational Waves from Phase Transitions in Models with Charged Singlets*, *Phys. Lett. B* **789** (2019) 119–126, [[1809.09883](#)].
- [79] J. Bernon, L. Bian, and Y. Jiang, *A new insight into the phase transition in the early Universe with two Higgs doublets*, *JHEP* **05** (2018) 151, [[1712.08430](#)].
- [80] T. Biekötter, S. Heinemeyer, J. M. No, M. O. Olea-Romacho, and G. Weiglein, *The trap in the early Universe: impact on the interplay between gravitational waves and LHC physics in the 2HDM*, *JCAP* **03** (2023) 031, [[2208.14466](#)].